I&EC research
Industrial & Engineering Chemistry Research

Review

Cite This: Ind. Eng. Chem. Res. 2019, 58, 16018−16032

pubs.acs.org/IECR

Multiscale Modeling of (Hemi)cellulose Hydrolysis and Cascade Hydrotreatment of 5-Hydroxymethylfurfural, Furfural, and Levulinic Acid

Rok Šivec, Miha Grilc,*,† Matej Huš,* and Blaž Likozar

†Department of Catalysis and Chemical Reaction Engineering, National Institute of Chemistry, Hajdrihova 19, 1000 Ljubljana, Slovenia

ABSTRACT: Numerous research studies have recently demonstrated a huge physical potential of the cascade companies' utilization of the renewable waste ligno-cellulosic biomass sources by the fractionation, de-polymerization and valorization of cellulose, hemicellulose, and lignin, separation, and subsequent catalytic conversion of the monomeric building blocks to biofuels, bio-based chemical substances and biomaterials. 5-Hydroxymethylfurfural (5-HMF), levulinic acid (LA) precursors, and furfural (FUR) are, in most characteristic platform compound compositions, produced by the water-mediated acidic hydrolysis of furans, pentose, and hexose carbohydrate sugars, which can be hydrogenated, oxidized, or dehydrated. These processes were subjected to surprisingly many systematic modeling applications on various operation scales. However, only a limited representative number of works managed to link any of atomistic- (ab initio density functional theory (DFT)), meso- (kinetic Monte Carlo (KMC), mean-field mechanistic rate micro-kinetics and diffusion) or macroscales (computational fluid dynamics (CFD), process model simulations and techno-economics), or integrate them together with classical equipment environment engineering tools (reaction energy thermodynamics, optimizing heat, momentum and mass balances and applicative reactor design). This Review article highlights the integration of interface chemistry methods as an emerging development approach that allows linking the insights about the molecular level measurements with elementary surface steps, while further with diffusive/convective transfers and process integration.

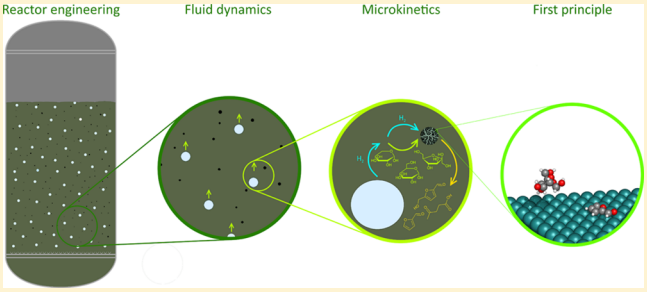

1. INTRODUCTION

Development of energy- and resource-efficient processes to convert renewable sources into platform chemicals or biofuels has become one of the major challenges in chemical engineering. There are many available thermo-chemical routes to valorize lignocellulosic biomass (Figure 1) and its constituents, namely hemicellulose, cellulose, and lignin, into liquid or gaseous energy carriers and platform chemicals that can be further converted into value-added drop-in chemicals and biopolymers.[1−7] Relatively simple hydrolysis of cellulose and hemicellulose yields pentoses (C_5) and hexoses (C_6) that are further dehydrated to 5-hydroxyfurfural (5-HMF), levulinic acid (LA), and furfural (FUR). These three compounds are considered to be among the most important biomass-derived platform chemicals and are also highlighted in Figure 2.[8,9] Due to the co-presence of several functional groups, 5-HMF, LA, and FUR can be further converted into a broad array of products and functionalities (Figure 3).[3,5] However, only some transformations were studied with the methods of theoretical chemistry or microkinetic modeling (MKM) investigations (red reaction arrows in Figure 2). In some cases (reaction with the dashed arrow), furfural was reported to be directly converted into 2-methylfuran, while in most studies furfuryl alcohol was proposed as an intermediate. As studies are not directly comparable, it is impossible to make a general conclusion.

Further attempts at linking atomistic scales, mesoscales, and macroscales of modeling are sparse but still relatively well covered compared to other catalytic reaction systems beyond the complexity of C_1 chemistry.

In order to better understand, describe, optimize, and predict the behavior of catalytic reactions in complex systems, multiscale modeling is a valuable tool, especially when applied complementary with a systematic experimental work. Biomass conversion on a large scale faces several important and unsolved practical challenges related to the reactor design and optimization of operating parameters or material properties of catalysts. Formation of non-volatile humins during the dehydration of hexose and pentose sugars to 5-HMF and FUR is still burdening the profitability of their large-scale production. Furthermore, degradation tendency of bio-based compounds is

Special Issue: Biorenewable Energy and Chemicals

Received: February 20, 2019
Revised: April 17, 2019
Accepted: April 23, 2019
Published: April 23, 2019

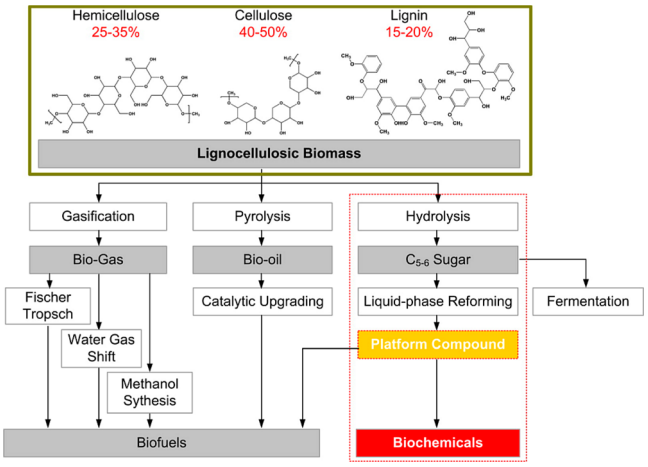

Figure 1. Different lignocellulosic biomass conversion options. Reprinted with permission from ref 10. Copyright 2016 American Chemical Society.

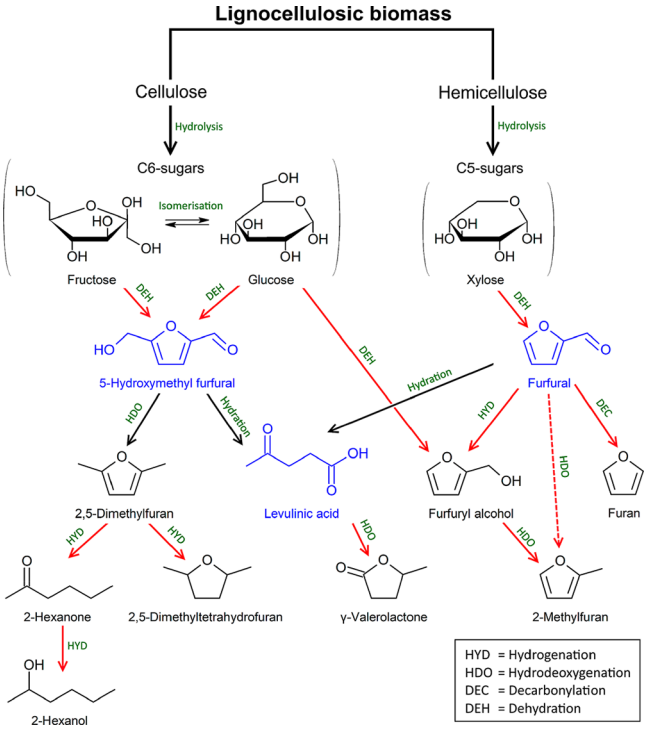

Figure 2. Main lignocellulosic biomass hydrolysis products (blue) and reactions considered in this Review. Those reactions supported by MKM are marked in red. The dashed arrow represents the reaction occurring only via surface intermediate species.

known to be responsible for a chemical deactivation of active site or their physical inaccessibility. In order to fully optimize the efficiency of a complex catalytic process, it is necessary to understand chemical reactions on a molecular level. Therefore, a mechanistic approach, describing each elementary step of the transformation(s), is necessary. As such equations describe the system on a much more fundamental scale compared to conventional models and take realistic (not apparent) kinetic parameters into account, it takes less experimental effort to identify and overcome the reaction bottlenecks. Furthermore, fine-tuning of reaction conditions for a specific objective (i.e., based on yield or selectivity, allowable operating conditions, or costs) is drastically simplified. Due to mechanistic understanding of every physical or chemical step or phenomenon, it is also easier to extend or link the model to different systems or scales. In contrast to traditional kinetic models used in chemical engineering, where apparent rate constants are usually determined, multiscale models can be used on a broader (ideally atom-to-process) scale, following a bottom-up or a top-down approach. The drawback of MKM, which is based on mechanistic understanding, is that the model can soon become too complex, and more caution is needed. Different methods for estimating reaction rates on a catalyst surface through a multiscale approach have already been reviewed by Salciccioli et al.[11] First principles-based modeling of catalytic gas-phase reactions (NO oxidation, CH_4 steam reforming, CO oxidation, etc.) was performed, while also highlighting the possibility of modeling reactions of more complex molecules in liquid media, for example, homogeneous HCl-catalyzed fructose conversion to 5-HMF. Other examples of catalytic biomass conversion reactions were lacking, as they were developed only in recent years. This motivated us to write this Review.

In most cases, *ab initio* studies consider only gas-phase reactions, where electronic structures are calculated at 0 K, 0 bar, and without considering solvent effects. With the development of analytical and computer technology, it is now possible to use first-principle methods to describe molecular level interactions even on a catalyst surface. Density functional theory (DFT) calculations have become one of the standard methods to describe and understand such phenomena, giving information on the kinetics and thermodynamics of catalytic surface reactions.[11]

As it is difficult to predict all possible reaction routes, it is still not realistic to perform DFT calculations for every intermediate in a very complex reaction system. It was estimated that over 10^4 reactions of only FUR and its derivatives can occur on a single metallic surface.[12] As DFT calculations come with a high computational cost, one has to use chemical intuition to study only the relevant reaction routes while still taking all the important variables into account. If this is not the case, accuracy of the calculations is questionable.

In addition to quantum chemical calculations (mostly DFT), a stochastic mesoscale approach can also be used—for instance, *ab initio* kinetic Monte Carlo (KMC) simulations. As KMC is known to be computationally less efficient than conventional mean-field MKM, it is not used as often.[13] It has been only recently shown that KMC can be used for the calculation of complex surface reactions by coupling multiscale modeling with active machine learning for computation of complex structure-dependent interactions on catalyst surfaces with low computational cost.[14]

More often, the obtained *ab initio* data are therefore used in a mean-field MKM, where the reaction rates are usually determined using the transition state theory (TST) on first-principles data.[15] Reaction rates are calculated, and the model can be fitted to experimental data for validation. It is important to account every surface phenomenon, including adsorption and desorption rates. By doing so, rate-limiting steps can be recognized which helps us achieve better conversion and selectivity. The data can also be used for catalyst design, screening, and operating conditions optimization.[16] With the addition of computational fluid dynamics (CFD), heat, and mass-transfer studies, a large-scale reactor can be designed through a multiscale approach (Figure 4).

Despite a huge potential of biomass-derived 5-HMF, LA, and FUR, their subsequent hydrotreatment processing, and the

DOI: 10.1021/acs.iecr.9b00898
Ind. Eng. Chem. Res. 2019, 58, 16018−16032

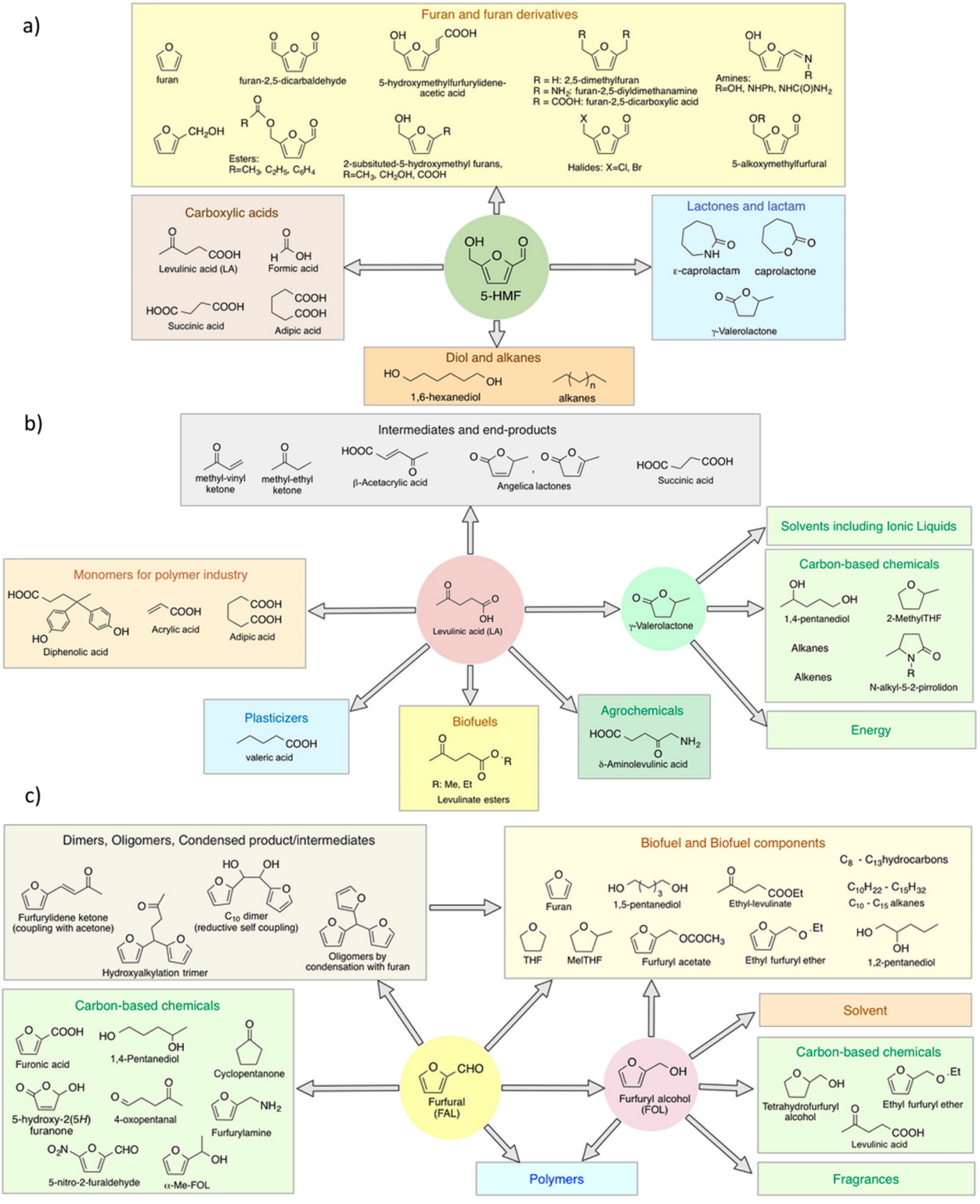

Figure 3. Possible derivatives of (a) 5-HMF, (b) LA, and (c) furfural. Reprinted with permission from ref 3. Copyright 2018 American Chemical Society.

corresponding value-added chemicals, these rather complex systems were studied only by a few authors who demonstrated a vertical integration of at least two calculation scales. The investigated systems differ in the use of solvents, catalysts, process conditions, and calculation methods; therefore, these interesting studies are challenging to critically review and compare, which was the main motivation for us to conduct this work.

2. LITERATURE REVIEW

In this Review, all the important multiscale models of biomass hydrolysis to 5-HMF, LA, and FUR and their hydrogenation (HYD), hydrodeoxygenation (HDO), decarbonylation (DEC), and oligomerization (OLIG) to value-added products are summarized in Table 1.

DOI: 10.1021/acs.iecr.9b00898
Ind. Eng. Chem. Res. 2019, 58, 16018−16032

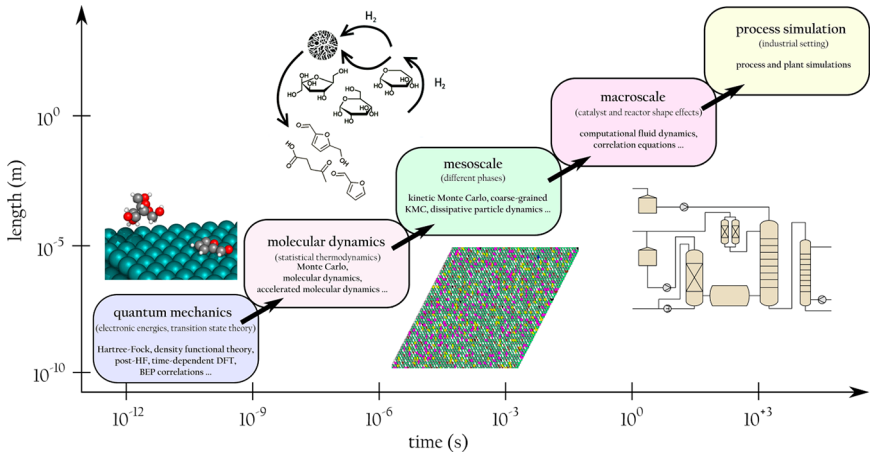

Figure 4. Different levels of multiscale modeling, from quantum mechanics to process simulation.

2.1. 5-Hydroxymethylfurfural. 5-HMF is a platform chemical derived from cellulose and hemicellulose. Chemically, it can be viewed as a derivative of fructose. Fructose is an isomer of glucose, which can form under catalyzed or non-catalyzed conditions. When fructose assumes a five-membered ring conformation (fructofuranose), it converts into 5-HMF in a series of three sequential dehydrations. It has been known since 1875 that 5-HMF is an intermediate in the conversion of sugars into LA.[34] As described in more detail later on, LA is formed through ring opening when 5-HMF is hydrated.

Several kinetic studies of 5-HMF production from biomass have been conducted, but most eschew a mechanistic explanation.[35] Mostly, the authors studied the mechanism of glucose and fructose conversion to 5-HMF and the hydrogenation of 2,5-dimethylfuran (DMF) to 2,5-dimethyltetrahydrofuran (DMTHF) using MKM.

Caratzoulas and Vlachos[17] studied the reaction mechanism and the rate of acid-catalyzed dehydration of D-fructose to 5-HMF in water with a hybrid quantum mechanics/molecular mechanics (QM/MM) approach. In this reaction, they modeled a proton and hydride transfer between the two molecules (Figure 5a). An intramolecular hydride-transfer step prior to the third dehydration step was found to be rate-determining, with a high free energy barrier of 31.8 kcal mol^{-1} on the account of reorganization of the polar solvent environment and the solvation of asymmetrical electronic charge contributions. The reported values is close to the experimentally determined activation energy of 33.7 kcal mol^{-1} in zeolites by Moreau et al.[36] The authors showed that in a medium with a lower dielectric constant, the reaction rate would increase. The overall reaction was found to be exothermic with ΔG = −20.5 kcal mol^{-1} at 90 °C. This value differs from the theoretical calculations (ΔG = −32.4 kcal mol^{-1}) by Assary et al.[37] on the G4 theory (B3LYP/6-31G(2df,p)) level. Assary et al.[38] later reported a theoretical value of −35.9 kcal mol^{-1} for the reaction free energy.

Nikbin et al.[18] continued this work and further refined the energetics of some elementary steps (Figure 5b). The calculated first-principles kinetics were used in a MKM, which they embedded in a classical kinetic model of a larger reaction network by Asghari and Yoshida.[19] While the standard approach of calculating the reaction rates of individual elementary steps using generalized Eyring equation mostly sufficed, they found out that the kinetic constant for the hydride-transfer steps require the Marcus theory to correctly describe the temperature dependence. Although the Marcus and Eyring theories lead to the same exponential form of the rate equations, the former must be used to describe the reactions without a noticeable structural change where the reactants change their charge. Hydride transfer is an example of such a reaction.

The apparent activation energies and the pre-exponential factors were fitted to the experimental data of Asghari and Yoshida.[19] A hydride-transfer step (R3 in Figure 5a) was found to be rate-determining due to the tunneling constant. However, another hydride transfer step (R6 in Figure 5a) was also found to influence the reaction rate significantly on the account of its highest Gibbs free energy. The results are in good agreement with experimental data over a wide temperature and reaction time range. The authors further note that, for a proper description of the reaction in aqueous environment, the transmission coefficient κ should be used in the transition state theory to compensate for the fact the TST was developed for gaseous-phase chemistry. This coefficient accounts for friction according to the theories of Kramers[39] and Grote−Hynes.[40]

Yang et al.[20] developed a mean-field MKM to describe the dehydration of glucose to 5-HMF, LA, furfuryl alcohol (FAL), and formic acid (FA), which is catalyzed by Brønsted acid sites. In contrast to classical kinetic studies,[41−43] they supported the mechanism by DFT calculations and experimental data (isotopic tracing). The first dehydration step of (protonated) glucose was identified to be rate-determining and strongly influenced by temperature and pH. The model accounts for two furanosyl intermediates (A in B), which can form via dehydration of protonated glucose, as shown in Figure 6. The isomerization reaction of glucose to fructose was also considered, but was found to have a negligible reaction rate (thin dashed line) in comparison to the consumption rate of glucose. Thus, two different paths ensue. In the first path (intermediate A), the first dehydration step has the highest apparent activation free energy (31.1 kcal mol^{-1}), which is consistent with experimental kinetic studies of Pilath et al.[42] In the second path (intermediate B), a similar apparent activation free energy of 31 kcal mol^{-1} is required. Through the formation of different intermediates (dashed lines), intermediate B can lead to the formation of FAL or 5-HMF (note that is the same as Intermediate 4 in Figure 5), according to the mechanism described before by Caratzoulas and Vlachos.[17] Comparing both routes, we see that the formation of 5-HMF is preferred. Glucose

DOI: 10.1021/acs.iecr.9b00898
Ind. Eng. Chem. Res. 2019, 58, 16018−16032

Table 1. All Multiscale Models of Biomass Hydrolysis Products Considered in This Review

							experimental							
substrate	reaction type	products	methodology	catalyst	first principles	meso-scale (microkinetics) conditions	reactor type	solvent	flow/volume/time	conditions	conversion	selectivity	remarks	ref
D-fructose	acid-catalyzed dehydration	5-HMF	QM/MM MD	H^+/H_2O	PM3 (reactive center) + SPC/E (bulk)	90 °C	N/A	N/A	N/A	N/A	N/A	N/A	semiempirical atomistic model used	17
D-fructose	acid-catalyzed dehydration	5-HMF, furfural, LA, FA	QM/MM MD, MKM, experiments	$HCl_{(aq)}$ (pH 1.3−2.3)	PM3 (reactive center) + SPC/E (bulk)	180−240 °C	plug-flow sub-CW reactor	HCl/H_2O	0.5−300 s residence time	190−270 °C, 4−15 MPa	<100%	<35% HMF, <35% LA, <35% FA, <4% furfural	hybrid QM/MM MD embedded in MKM	18, 19[a]
glucose	acid-catalyzed dehydration	5-HMF, LA, FA, FAL, side products, condensation products	DFT, MKM, experiments	H^+	B3LYP/6-31+G(d,p), two explicit water molecules + CPCM	140−180 °C	batch reactor	HCl/H_2O	10 mL, 0−150 min	140 °C	<100%	<10% HMF, < 25% FA, < 20% LA	NMR spectroscopy and isotope labeling included	20
DMF, MFL, MFA	HYD, HDO, ring opening	DMTHF, 2-hexanol, 2-hexanone, 2,5-hexanediol	DFT, MKM, experiments	Ru/C; four-layer Ru(0001)	PBE + D3	55−80 °C (DMF), 170−200 °C (MFL/MFA)	batch reactor	2-propanol	50 mL, 0−120 min	80 °C, 20.67 bar	<99%	<73% DMTHF, < 19% 2-hexanol, < 1% to 2-hexanone	microkinetic data not compared with experimental	21
LA	HDO, DEC, OLIG	GVL, butanone, butanol, dimers, pentanoic acid, pentenoic acid	MKM, experiments	sulfided $NiMo/Al_2O_3$	N/A	225−275 °C, 25−75 bar	batch slurry reactor with continuous gas flow	none	300 mL, 0−220 min	225−275 °C, 25−75 bar	<90%	<90% GVL	internal and external mass transfer included	22
LA	HYD, dehydration, ring closure (esterification)	GVL	DFT, MKM	four-layer Ru(0001)	PBE + D3	50−250 °C, 10 bar	N/A	N/A	N/A	N/A	100%	100% GVL	adsorbate−adsorbate interaction and BEP included	23
LA	HYD, dehydration, ring closure (esterification)	GVL, 4-hydroxy pentanoic acid (HPA)	DFT, MKM, experiments	four-layer Ru(0001)	PBE + D3	50−250 °C, 4−40 bar	packed-bed reactor	water	0−24 h, 5−1500 h^{-1} WHSV	50−150 °C, 4.1−41.5 bar	<99%	<81% GVL, <98% HPA	experimental data from ref 24	25, 24[a]
furfural	HYD, DEC	FAL, furan	DFT, MKM, experiments	four-layer Pd(111)	PBE + D3	180−300 °C, 0.1−1000 mbar, 8.257 cm^3/s	tubular flow reactor	95% unreactive diluent	0.5 mL/h, 0−60 min, 2 cm length, 4 mm diameter	210−250 °C, 1 bar (1:25 furfural:H_2)	<98%	18−70% furan, 8−72% FAL	hydrogen coverage effects included	26, 27[a]

Ind. Eng. Chem. Res. 2019, 58, 16018−16032
DOI: 10.1021/acs.iecr.9b00898

Table 1. continued

substrate	reaction type	products	methodology	catalyst	first principles	meso-scale (microkinetics) conditions	experimental						remarks	ref
							reactor type	solvent	flow/volume/time	conditions	conversion	selectivity		
furfural	HYD, DEC	FAL, furan	DFT, MKM, experiments	four-layer Pt(111) and Pt(211), Pt_{55} cuboctahedron	PBE, vdW-DF	170−245 °C, 102.3 (9.3−186) kPa	tubular fixed-bed reactor	N/A	1300 h^{-1} GHSV	170− 245 °C, 102.3 kPa (1:10 furfural:H_2)	100%	0−96% FAL, 8−82% FA, 15−92% furan	effects of steps and nanocluster studied	28, 29[a]
furfural	HYD, HDO (hydrogenolysis)	2-MF, FAL, dimers	DFT, MKM, experiments	Ru/RuO_x/C; three-layer RuO_2 (110) and Ru(0001)	PBE	140 °C, 2.04 MPa	batch reactor	10% 2-propanol in toluene; or *tert*-butyl alcohol	100 mL, 0−300 min	140 °C, 2.04 MPa	<37%	<8% 2-MF	DFT only for adsorption energies, no coupling with kinetics; isotope labeling	30
furfural, FAL	HYD with Mars−van Krevelen C−O activation	2-MF	DFT, MKM	four-layer Ru(0001) and RuO_2(110)	PBE + D3	140 °C, 3.49 MPa	N/A	N/A	N/A	N/A	<100%	<76% 2-MF	first low-temperature radical reduction mechanism in heterogeneous catalysis	31
furfural (*cis* and *trans*)	HYD, HDO, DEC	2-MF, furan, FAL	DFT, MKM, experiments	four-layer Mo_2C(101)	PBE + D3	150 °C, 1 bar	tubular quartz reactor	N/A	1.67 cm^3 s^{-1}, 10 mm inner diameter	150 °C, 0.1−1.0 bar	<13%	60−95% 2-MF, 0−35% dimers, 0−10% FAL	extensive investigation of coverage effects on the pathway	32, 33[a]

[a]Experiments from the second cited reference.

DOI: 10.1021/acs.iecr.9b00898
Ind. Eng. Chem. Res. 2019, 58, 16018−16032

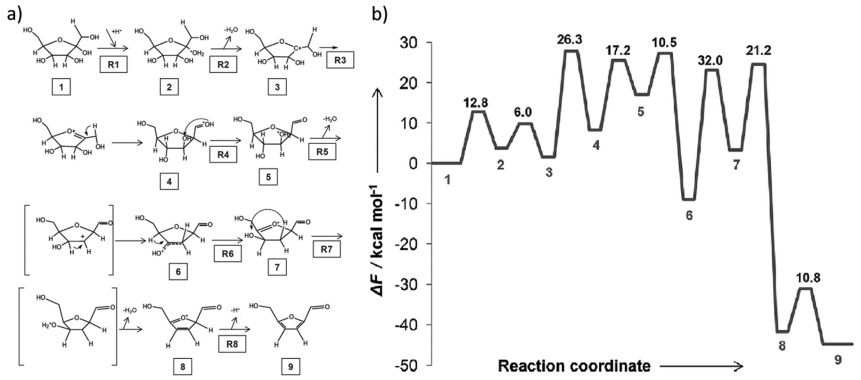

Figure 5. (a) Proposed mechanism of D-fructose dehydration to 5-HMF, with unstable intermediates in brackets, and (b) the corresponding (improved) free energy profile of D-fructose dehydration. Reprinted with permission from ref 18. Copyright 2012 John Wiley & Sons, Inc.

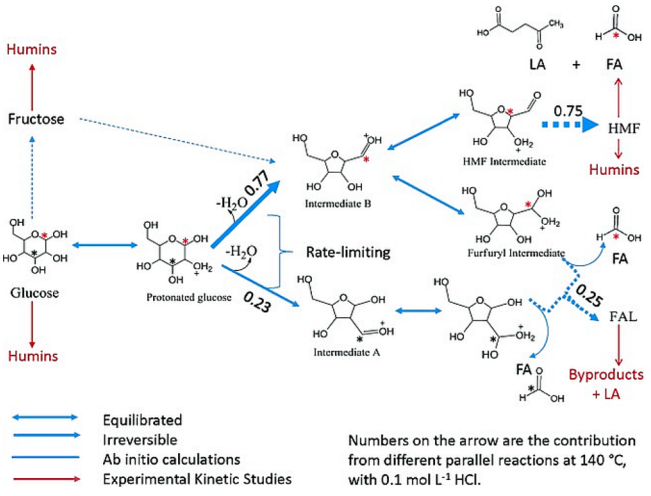

Figure 6. Reaction scheme of glucose dehydration, where the numbers on arrows represent the selectivity to parallel reactions at 0.1 mol L^{-1} HCl and 140 °C. Reprinted with permission from ref 20. Copyright 2015 John Wiley& Sons, Inc.

condensation (yielding disaccharides) was also considered and found to have an apparent activation free energy of ~20 kcal mol^{-1}. However, the reaction is endothermic with the free energy change of 15.6 kcal mol^{-1}. The contribution of this route at higher temperatures is negligible.

Gilkey et al.[21] studied the mechanism of DMF conversion over Ru/C catalyst by DFT calculations and microkinetics. It is known that 5-HMF can be hydrodeoxygenated to DMF[44−47] and then further converted into other value-added chemicals. Gilkey et al. also performed experiments with individual intermediates to map out the reaction network. Using isopropanol as hydrogen donor, they investigated the mechanism (Figure 7a) and energetics (Figure 7b) of two main parallel pathways: (a) ring opening, producing 2-hexanol (HOL) and 2-hexanone (HON), and (b) ring hydrogenation, producing DMTHF. During the reaction, a small amount (~3%) of isopropanol was converted mostly to acetone and hydrogen (~80%), but also to diisopropyl ether (~7%). They also identified two important intermediates as 2,5-dimethyl-2,3-dihydrofuran (DMDHF) and 2,5-hexanediol (2,5-HDL). With the addition of water, hydroxyl species formed on the Ru surface, leading to the formation of 2,5-HDL, which can further convert into DMTHF.

They also studied the steric effects of the solvent and the effect of side groups, beginning with 5-methylfurfural (MFL) and (5-methyl-2-furyl)methanol (MFA). An expanded reaction network can account for the formation of even more byproducts: 2-methylfuran (2-MF), 2-methyl tetrahydrofurfuryl alcohol, 2-methyl-5-[(1-methylethoxy)methyl]furan, 1,5-hexanediol, and 1,2-hexanediol. Extensive DFT calculations and MKM helped elucidate the energetics, structures, and surface coverages of the reaction, although they have not been coupled with experimental data. The authors showed that the Ru(0001) surface is mostly populated with 2-propoxy (0.67 monolayers (ML)), DMF (0.29 ML), and 2-propanol (0.03 ML). The activation barrier for ring opening is low enough for the majority of DMF to be present in an open-ring structure. This structure then preferentially hydrogenates and only then undergoes a ring closure, yielding DMTHF in the process (see Figure 7). DMF in the open-ring structure can also fully hydrogenate to 2-hexanone and 2-hexanol due to lower barriers for the formation of C−H bonds as opposed to O−H bonds. The authors performed DFT calculations on a clean surface and with a 0.75 ML of 2-propoxy species, which corresponds to the reaction conditions. Steric repulsion at such high coverages was found to be significant, decreasing adsorption interactions (for instance, from 2.12 to 0.66 eV for DMF). The effect on the reaction barriers was less pronounced, generally lowering the barriers as opposed to the clean surface.

Employing experiments, hybrid QM/MM calculations, and MKM, Patet et al.[48] studied the Diels−Alder cycloaddition of DMF and ethylene, followed by dehydrative aromatization, to produce *p*-xylene. The reaction was performed on H−Y zeolite catalysts (faujasite) with *n*-heptane as a solvent. The first step of the reaction, namely cycloaddition does not require a catalyst, while active Brønsted acid sites must be present for subsequent dehydration. The authors studied the corresponding regime change, brought about by the change of acid site concentrations. They showed that at low acid site concentrations, the p-xylene formation rate follows a linear dependence with regards to the concentration of strong Brønsted acid sites at tested temperatures (200 and 250 °C), as the concentration of acidic sites is the limiting factor. At high acid concentrations a catalyst-independent regime is discovered as Diels−Alder cycloaddition becomes the rate-determining reaction. The authors used their QM/MM calculations of adsorption energies and reaction barriers to construct a MKM, the results of which compared favorably with the experiments. In their further work, Patet et al.[49] carried out experiments and DFT and MKM calculations to study the Diels−Alder cycloaddition and dehydrative aromatization of furanics with

DOI: 10.1021/acs.iecr.9b00898
Ind. Eng. Chem. Res. 2019, 58, 16018−16032

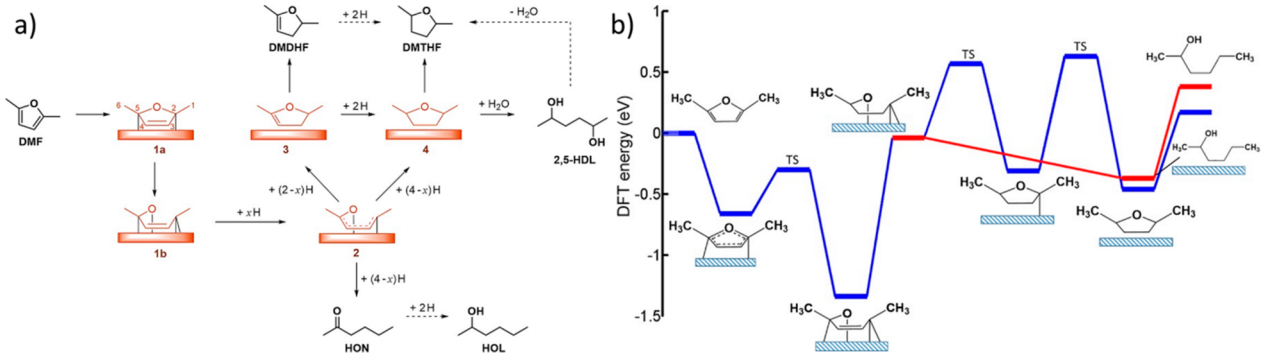

Figure 7. (a) DMF hydrogenation mechanism on Ru surface (drawn in orange). (b) DFT derived energy diagram with transition states for DMF conversion to DMTHF (blue) and HOL (red). Reprinted with permission from ref 21. Copyright 2016 John Wiley & Sons, Inc.

ethylene to aromatics in zeolites with varying metals (Al/BEA, Fe/BEA, Ga/BEA, and B/BEA). When 2-MF, furan, and DMF were used as reactants, benzene and *p*-xylene formed predominantly. Electronic structure calculations were used to parametrize a MKM which revealed that the reaction is not affected by changing the Brønsted acid strength of the zeolite catalyst, as also confirmed experimentally.

Green et al.[50] conducted experimental studies and kinetic and QM/MM calculations on the Diels–Alder cycloaddition of 2-MF and ethylene on H-BEA and Sn-BEA catalysts. The main product was toluene, albeit with rather low selectivity (<46%) on the account of dimerization, trimers formation, hydrolysis, and ring-opening of the reactant. Computationally, they studied the system on a hybrid QM/MM level with a mechanically embedded cluster model, which was used in a reduced model. The model was parametrized and fit to the experimental data.

Hočevar et al.[51] studied hydrogenation and hydrodeoxygenation of hexane, hexanone, and hexanol species (the =O and —OH groups at the second and third carbon atoms) on a sulfided NiMo/γ-Al_2O_3 catalyst in a three-phase slurry reactor. To describe experimental data, they developed a global MKM explicitly accounting for transport phenomena. In the model, conversion between intermediates is modeled in a lumped fashion, omitting unstable intermediates. However, DFT studies were also performed and used to show that the model values for activation barriers (not coupled in the model) are reasonable. The authors also studied the double bond migration and the corresponding *cis–trans* isomerization in C_6 olefins, which occurred also homogeneously (with catalyst). The HDO activity of different functional groups (ketone, alcohol) and double bonds at different positions were investigated in detail, using the model compounds approach. Based on first-principles modeling, the authors noted a distinction between sulfided active sites (for hydrogenation) and vacancy sites (for hydroxylation), but did not include this into modeling. Hočevar et al.[52] further investigated the HDO mechanism of primary C_6 species (with the functional groups on primary carbon atoms). Using the same methodology, hydrotreatment of 1-hexanol, hexanoic acid, methyl hexanoate, dihexyl ether, and hexanal was evaluated experimentally and in a MKM, while DFT results were used to supplement the model but did not feed into it.

As shown, different approaches can be used to mechanistically describe elementary reactions, but the methods should be carefully chosen, depending on case to case. The mechanism of fructose and glucose dehydration (by using a homogeneous acid catalyst) to 5-HMF was studied in detail by using hybrid QM/MM calculations and kinetics. Most elementary steps can be described by using the Eyring equation, while Marcus theory should be used for hydride transfer steps. A transmission coefficient in the TST, which accounts for friction, should offer a better description of reactions in aqueous environments. Experimental isotopic tracing experiments, coupled with DFT calculation and kinetics, could lead to convincing conclusions on reaction mechanisms. The reaction network can also be mapped out by using different intermediates as initial reactants, as was presented in the case of DMF conversion. A model compound approach was used to study the activity of different functional groups (ketone, alcohol) according to double bond positions. Most of the kinetic experiments were conducted in a kinetic regime, neglecting transport phenomena (which should be carefully proven). Including the latter, the MKM can have a broader use. In case of liquid reactions, the use of solvent should also be taken into account, as it can greatly influence the reaction by participating in the reaction, changing the orientation of molecules and surface species, occupying surface sites, and sterically or energetically influencing the adsorption/desorption of other species. By taking a look into a multiscale perspective, only examples of coupling quantum calculations, surface coverages with mass balances solved using differential equations were presented. Mass transport was also taken into account in a slurry batch reactor. In order to link the scales, MKM should be coupled with fluid dynamics, incorporating heat and mass transfer. Further integration of surface kinetics into a process simulation was also not yet found, even though some models are based on simple kinetic laboratory experiments to obtain kinetic parameters, further used as input parameters.[53]

2.2. Levulinic Acid. LA is claimed to be an *ideal platform chemical* due to its *gamma-keto acid functionality* and possible utilization to produce biochemicals (*resins, polymers, herbicides, pharmaceuticals and flavoring agents, solvents, plasticizers, antifreeze agents*) and biofuels or fuel additives.[54]

Its production from biomass is reported to be more sustainable and economically feasible in comparison to the traditional methods that involve petrochemical conversion of maleic anhydride.[54] It can be produced from cellulose and hemicellulose, through C_6 sugars and 5-HMF formation (Figure 2). It can also be converted from C_5 sugars through FUR formation, its hydrogenation to FAL, and subsequent dehydration.[54] While kinetics of LA production has been studied, none of these models were linked with molecular

DOI: 10.1021/acs.iecr.9b00898
Ind. Eng. Chem. Res. 2019, 58, 16018–16032

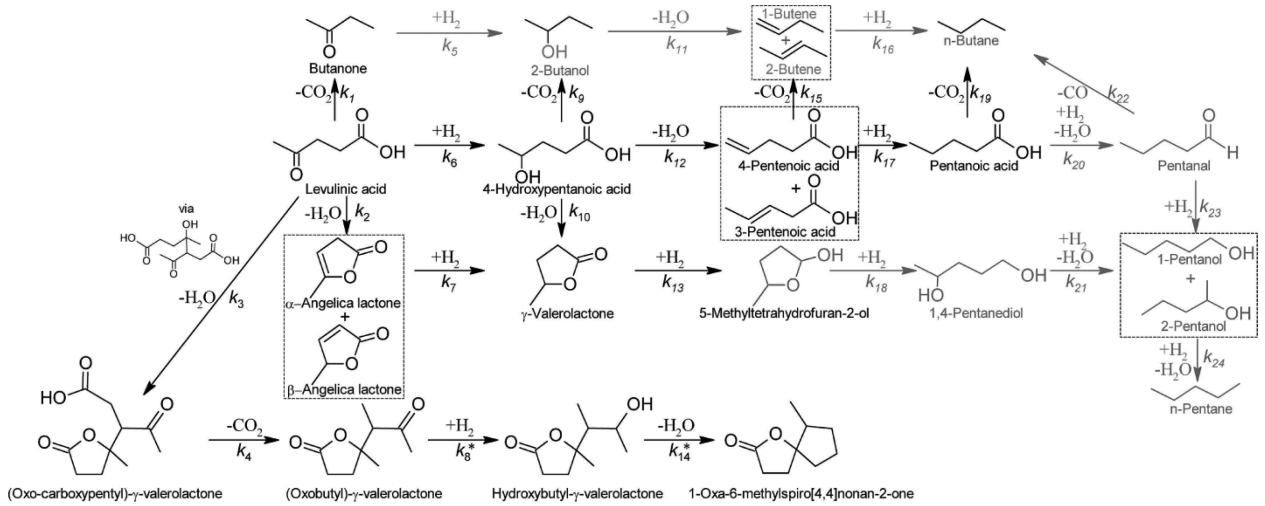

Figure 8. LA hydrogenation mechanism proposed by Grilc and Likozar.[22] Reprinted with permission from ref 22. Copyright 2017 Elsevier.

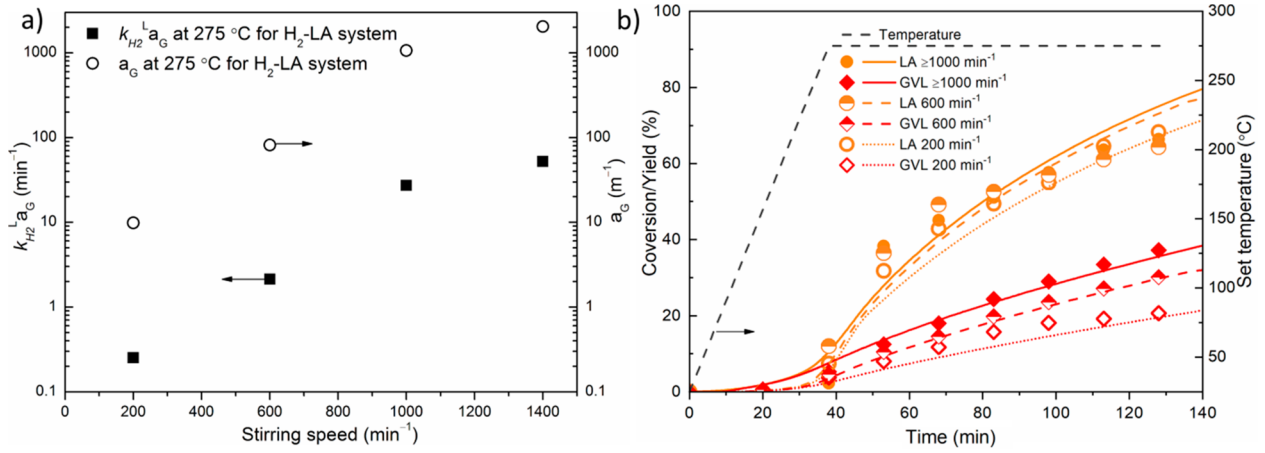

Figure 9. Influence of stirring speed on (a) the mass transfer coefficient and specific surface area of H_2 bubbles (taken from ref 22) and (b) the conversion of LA and yield of GVL. Reprinted (a) or adapted (b) with permission from ref 22. Copyright 2017 Elsevier.

dynamics simulations.[7,41,43,55−62] By means of MKM, most of the authors studied only the mechanism of LA hydrodeoxygenation to γ-valerolactone (GVL).

Grilc and Likozar[22] studied LA conversion in a three-phase batch slurry reactor by following a complex catalytic mechanism (Figure 8) over a sulfided $NiMo/Al_2O_3$ catalyst at solvent-free conditions, with a continuous flow of fresh H_2 or N_2. With this MKM, the influences of temperature, pressure, catalyst loading, and internal and external mass-transfer limitations were well described as kinetic rate constants and activation energies were determined for 24 reactions. The model is based on regression analysis of experimental results, where temperature, pressure, stirring speed, catalyst mass fraction, and catalyst particle size were successively varied. This approach allows to independently study the reaction kinetics in kinetic regime, when internal (small catalyst particles) and external (high stirring speed) mass transport can be neglected, or in a regime where mass-transfer limitations significantly affect the global reaction rate(s). The reaction in most cases took place in the kinetic regime, as further particle size reduction and higher stirring speeds had no effect on concentration profiles of reactant, intermediates, and products. Above stirring speed of 1000 min^{-1} surface reaction rates were much slower than mass transfer for all grain sizes of 1.2 mm or less, as mass transfer coefficient became very high and changes in concentration profiles became negligible (Figure 9). The solvation of reactant gas, transport in the bulk liquid, and further adsorption and desorption to the catalyst surface have to be accounted for in order to properly incorporate mass-transfer phenomena to the kinetic model. In such a way, parameters for intrinsic kinetics at different conditions can be used and directly compared to DFT calculations. Four important pathways were identified. The desirable reactions yielding GVL take place via angelica lactone (less dominant) or 4-hydroxypentanoic acid (HPA) formation (dominant). Competitive parasitic reactions, such as decarboxylation to 2-butanone or oligomerization followed by dehydrative cyclization, leading to oxo-carboxypentyl-γ-valerolactone, were mainly non-catalytic. They took place in a bulk liquid and are not to be neglected, especially at higher temperatures (their activation energy being significantly higher compared to catalytic HDO). It has been demonstrated that the stirring speed has an important effect on gas hold-up, which can crucially induce the influence of mass transfer resistance on a global rate of catalytic reactions (Figure 9), which should also be taken into account by other authors.[22] The most desirable reaction temperature was found to be 225 °C, where GVL was produced with nearly perfect selectivity via LA hydrogenation

DOI: 10.1021/acs.iecr.9b00898
Ind. Eng. Chem. Res. 2019, 58, 16018−16032

to HPA, followed by the dehydrative cyclization. LA hydrogenation was identified as the rate-limiting step. On the other hand, Mamun et al.[25] attributed the rate-determining step even before the formation of HPA, by the elementary step of alkoxy group formation on Ru(0001) catalyst.

Mamun et al.[23] also reported a theoretical study focused on the mechanism and microkinetics of LA conversion to GVL. Different reaction pathways with and without HPA formation were studied. Two adsorption mechanisms were also compared: specifically, a competitive one-site adsorption mechanism, where all species can adsorb on all sites, and a two-site mechanism, where one type of sites is accessible only to hydrogen and the other type is accessible to all other molecules. The model can predict the behavior of Ru(0001) catalytic surface reactions at medium temperatures (150−250 °C), where a discrepancy of a turnover frequency (TOF) within 1 and 2 orders of magnitude (being within the DFT calculations error) was observed after a comparison with experimentally based data of Braden et al.[63] A larger deviation occurs at lower temperatures (50 °C), as the catalyst surface seems to be inactive for the proposed reaction due to low availability of vacant active sites. Experimental data of Abdelrahman et al.[24] show TOF being 6 orders of magnitude higher than the model prediction; however, an eventual positive effect of aqueous media on the reaction rate was not taken into account in MKM. LA adsorption and the first hydrogenation step to alkoxy intermediate with an activation barrier 64.45 kJ mol^{-1} have been identified as the rate-determining steps. For the calculation of elementary surface rate constants, they used the Eyring equation according to harmonic transition state theory.

In order to further investigate this reaction, Mamun et al.[25] added the second route of GVL formation through α-angelica lactone intermediate using the one-site and two-site models. The most favorable pathway for LA hydrogenation to GVL in a nonpolar media remains via alkoxy intermediate formation, while routes involving angelica lactone and HPA formation are not plausible. The two-site model type predicts that some derivatives of angelica lactone can poison the catalyst surface at temperatures above 150 °C, while the one-site model shows that hydrogen causes poisoning at low temperatures. The authors explicitly accounted for lateral interactions between the adsorbed hydrogen atoms to prevent the catalyst surface from unrealistically high saturation with hydrogen. This alone would artificially increase the oxygen surface coverage, necessitating the incorporation of H−H, O−H, and O−O lateral interactions in the model. The coverage of other species is low enough; therefore, the introduction repulsion effect was not required in the model. Comparison to experimental data leads to the same conclusion; even as the results of both models are in agreement with experimental data at temperatures above 150 °C, the modeled TOF is underestimated at lower temperatures (50 °C). This leads to the conclusion that Ru(0001) sites are probably not responsible for LA hydrogenation at these conditions, due to solvent effects, which were not taken into account, or due to the activity of other Ru surface sites on Ru(100) and Ru(101) crystal planes. Nevertheless, further studies are needed in order to understand the complete mechanism.

Abdelrahman et al.[64] studied the hydrogenation microkinetics (based on Horiut−Polanyi mechanism and an analysis based on Langmuir−Hinshelwood mechanism, with two distinct surface sites) of C_3 to C_5 ketone species (acetone, 2-butanone, and 2-pentanone) on Ru/SiO_2 catalysts over a range of ketone and hydrogen partial pressures at different temperatures. The MKM was supported by experiments and DFT study. The kinetic parameters of the rate-determining step (addition of a hydrogen atom to the surface alkoxy species) was proposed to be almost independent of the chain length with value of the pre-exponential factor $\sim 10^{11}$ s^{-1} and an energy barrier of 66 kJ mol^{-1}. Furthermore, total TOF has experimentally decreased with chain length, proposedly due to higher surface coverage of adsorbed molecules (multiple sites covered by a single adsorbed molecule). This should also apply to LA, as the energy barrier is close to that reported by Mamun et al.,[23] and hydrogenation rates in water were reported to be the same as those of 2-pentanone.[65]

By using MKM and experimental testing, Bond et al.[66] studied further gas-phase conversion of GVL. They investigated the ring opening (to pentenoic acid isomers), reversible ring closure, and subsequent decarbonylation (to butene isomers) mechanism by using amorphous silica−alumina catalyst in a down-flow fixed-bed reactor. The MKM is based on thermodynamic calculation, suggesting gas-phase carbenium and oxonium ions as intermediates. The mechanism is described by pseudo-elementary steps, where pentenoic and butene isomers were treated as lumped species. Due to lack of data, the model follows many simplifications, but the concept of using a Born−Haber thermochemical cycle to describe heats of adsorption, which separately takes thermodynamic data for gas molecules, surface species, and specific catalyst surface sites into account, could lead to a deeper fundamental understanding. This makes it easier to calculate the heat of adsorption of a specific molecule to any solid acid catalyst surface site by changing only deprotonation energy values of the latter. Free energies of elementary reaction also give insight into surface coverages of individual species at equilibrium. The reaction was proposed to be limited by a surface reaction, even though no specific rate controlling step was found.

Other multiscale models are sparse and/or follow only simplified kinetics. Chung et al.[67] for instance, presented a model which includes simple kinetics of LA and *n*-butanol esterification to *n*-butyl levulinate by using a homogeneous catalyst (sulfuric acid) in a reactive distillation system with the goal of finding the most economical process heat and mass transfer. The kinetic and distillation parameters were used to find an optimal design for the reactive distillation column, while operating at different conditions (pressures from 1 to 17 bar). To get a more realistic picture, the model was integrated into a process simulation including heat and mass transfer. A process control strategy was also proposed.

Kokare et al.[68] conducted a study of *n*-butyl levulinate synthesis by using levulinic acid, *n*-butanol, and Amberlyst 15 catalyst. Kinetic experiments were performed by excluding external and diffusional mass transfer, following a design of experiments concept. A central composite design with response surface methodology was used. Empirical correlations and a Langmuir−Hinshelwood−Hougen−Watson model were used to describe pseudo-homogenous intrinsic kinetics, followed by a process flow sheet simulation which includes the optimization of reactive distillation. Reaction parameters (acid to alcohol molar ratio, catalyst loading, and temperature) were optimized. A process setup with the use of two columns for separation was compared to the use of a reactive divided wall column, where the latter proved to be more economical. A 97% conversion was estimated after a reaction time of

DOI: 10.1021/acs.iecr.9b00898
Ind. Eng. Chem. Res. 2019, 58, 16018−16032

75 min at 397 K, using 20 wt% catalyst loading and molar ratio of 1:4 (LA to *n*-butanol).

In most cases, the mechanism of catalytic conversion of LA to GVL on a solid catalyst was studied. Some authors studied the mechanism in more detail, following all possible surface intermediates, while others included a broader scale, leading to different intermediates and products, while following different reaction routes. For instance, homogeneous reactions follow a different mechanism as reactions occurring on catalyst surfaces. When conducting reactions in multiple phases, gas−liquid transport phenomena and liquid−solid mass transport needs to be accounted for (or proven otherwise). With the use of elementary reactions, the reaction network can be expanded as needed. It was determined with MKM that some discrepancies can occur at lower or higher temperatures. If such anomalies occur, it is worth accounting for lateral interactions between adsorbed molecules (e.g., in case of unrealistic hydrogen saturation at lower temperatures). In most DFT based models, authors only consider one surface plane of the catalyst to be active for the reaction, but surfaces have different geometries which also include other crystal planes, border sites, and vacancies which can all have influence on the reaction. A different approach, using thermodynamic calculations coupled with MKM was also shown to be a promising, fundamental approach, but there is a lack of thermodynamic data in the literature. Some modeling on a larger scale was found, but such models follow very simplified kinetics or empirical correlations, which are based solely on a few lab-scale experimental results.

2.3. Furfural. FUR is another important platform chemical, which can be obtained from biomass. When hemicellulose present in lignocellulosic biomass is hydrolyzed, C_5 sugars are also obtained. Acid-catalyzed sequential dehydration (−3 H_2O) of a pentose (for instance, xylose) yields FUR.[26] Reactivity of FUR has already been extensively studied, but research has focused mostly on experiments, often lacking a detailed mechanistic understanding. Nevertheless, a few microkinetic models describing the kinetics of FUR conversion have been developed. The selectivity in FUR conversion is strongly dependent on the catalyst used, which in turn influences the conformation of adsorbed species, and on the operating conditions.

Wang et al.[26] studied FUR conversion computationally and developed a DFT-based MKM, focusing on hydrogenation and decarbonylation (Figure 10) of FUR on platinum. Using DFT calculations, they studied elementary reaction steps for the reaction with low 0.5, and 0.75 ML hydrogen coverage on Pt(111). Also, its own coverage strongly influences the adsorption mode of FUR. At higher coverages, the adsorption mode of FUR changed from flat to tilted, which resulted in a large change of adsorption energy (from 1.96 to 1.00 eV) and activation barriers. This change of conformation significantly affected the selectivity of the reaction and TOF. The reaction can be thus steered differently by varying the experimental conditions. The hydrogenation reaction (leading to FAL) is favored at higher hydrogen pressure and consequently coverage (FUR in tilted orientation), while decarbonylation (leading to furan) occurs at lower hydrogen pressure (flat orientation of FUR). Lower temperatures lead to higher selectivity toward FAL, but they also lower the reaction rate. As temperature has minor influence on selectivity in comparison to hydrogen pressure, the selectivity should be tuned by adjusting the pressure while keeping the temperature high enough to achieve desired reaction rates at acceptable

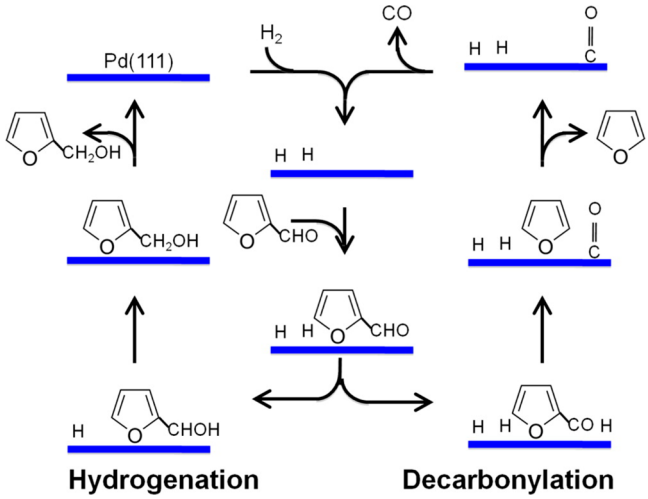

Figure 10. Considered hydrogenation and decarbonylation reactions in the MKM of Wang et al.[26] Reprinted with permission from ref 26. Copyright 2014 American Chemical Society.

selectivity. Figure 11 shows that as the adsorption is stronger at lower hydrogen coverages, the overall potential energy surface is shallower at higher hydrogen coverage. Activation barriers for hydrogenation and decarbonylation are the lowest at moderate hydrogen coverages.

Cai et al.[28] computationally investigated the effect of different surface motifs of platinum on FUR conversion. Extensive DFT calculations of FUR hydrogenation and decarbonylation were performed and the results embedded in a MKM model. The authors studied the reaction on a flat Pt(111) surface, on a stepped Pt(211) surface, and on a Pt_{55} cluster. The effect of particle size in correlation with the concentration of individual surface sites as proposed in literature[70,71] was also included in the model. The effect of the structure of active sites was revealed to be large. The authors showed that hydrogenation is preferred on larger Pt particles (>1.4 nm), while smaller ones (<1.4 nm) favor the decarbonylation route. Despite being a theoretical study, parallels with external experimental data were drawn. The particle size effect on the selectivity (Figure 12a) trend was found to be comparable to the experimental data of Pushkarev et al.[29] (Figure 12b). The model was used to predict a correlation to the concentration of individual surface sites only on cuboctahedral-shaped Pt particles, which is not necessarily the case in experiments. While Pt_{55} sites are well suited for selective decarbonylation, the formation of FAL is favored at low temperatures as the Pt_{55} nanoclusters are subject to CO poisoning (which desorbs at higher temperatures). The nanocluster is fully covered with CO below 443 K. With the increase of temperature, the formation of furan also becomes dominant on the Pt(211) surface sites.

Gilkey et al.[30] studied the mechanism of FUR hydrogenation in a combined theoretical and experimental study. The conversion of FUR to 2-MF proceeded via the formation of FAL with isopropanol as a hydrogen donor over a bifunctional $Ru/RuO_x/C$ catalyst. The authors showed the hydrogenolysis of FAL to be limited by the rate of the C−H bond scission rather than the C−O bond cleavage. FAL is formed primarily via the Lewis acid-catalyzed intermolecular hydride transfer from isopropanol to FUR on the Lewis acid sites of RuO_x via the Meerwein−Ponndorf−Verley mechanism. The major pathway leading to 2-MF was found to be aromatic ring

DOI: 10.1021/acs.iecr.9b00898
Ind. Eng. Chem. Res. 2019, 58, 16018−16032

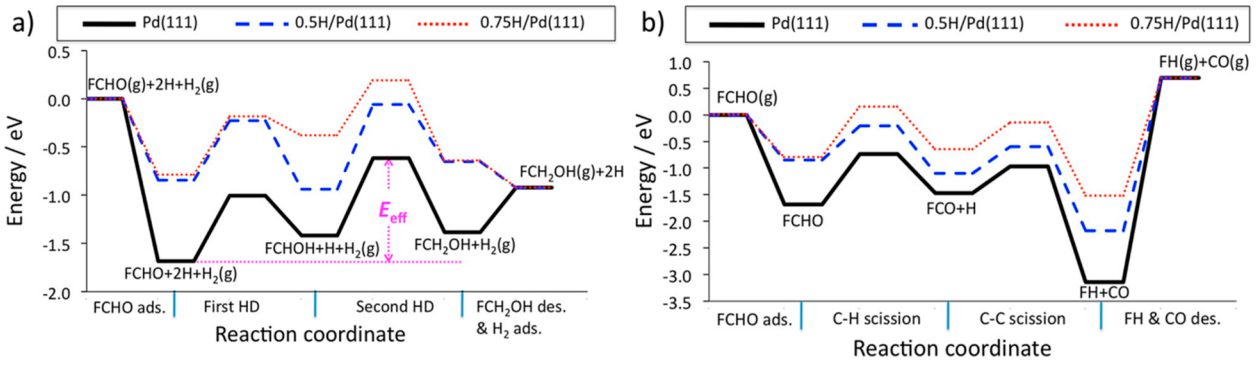

Figure 11. Energy profile at different coverages of hydrogen for FUR (a) hydrogenation to furfuryl alcohol and (b) decarbonylation to furan, as proposed by Wang et al.,[26] where data for clean Pd(111) surface were taken from ref 69. Reprinted with permission from ref 26. Copyright 2014 American Chemical Society.

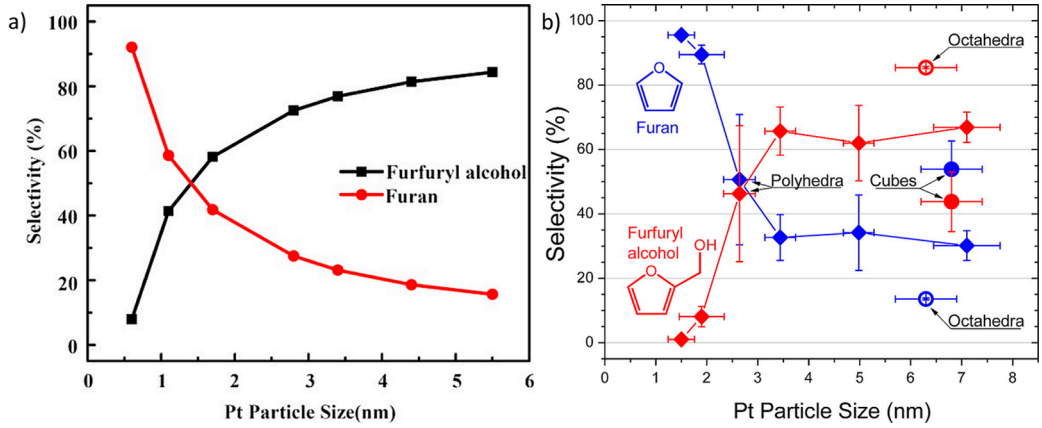

Figure 12. Selectivity to furfuryl alcohol (FAL) and furan versus the Pt particle size at 93 kPa H_2, 9.3 kPa FUR, and 473 K. (a) Values predicted by the model of Cai et al.[28] and (b) values experimentally determined by Pushkarev et al.[29] Panel (a) reprinted with permission from ref 28. Copyright 2015 by John Wiley & Sons, Inc. Panel (b) reprinted with permission from ref 29. Copyright 2012 American Chemical Society.

activation rather than direct dihydroxylation and hydrogenation on metal sites. They also observed that reversible etherification can occur between isopropanol and FAL.

Mironenko and Vlachos[31] explained why certain multifunctional metal/metal oxide catalysts exhibit high C−O scission activity even at moderate or low temperatures. They studied this reaction on FAL (hydrogenolysis of FAL), showing that a mix of Ru(0001)/RuO_2(110) surfaces produces high selectivities and yields. Based on extensive DFT calculations and an overarching MKM, formation of 2-MF below 200 °C was observed. The synergistic effect has a two-fold origin: on RuO_2 oxygen vacancies C−O bond activation is mediated by radicals, while on Ru(111) hydrogenation occurs. The Ru metal is responsible for the regeneration of vacancies and higher dissolved hydrogen concentration. On the other hand, RuO_2 is responsible for catalysis of hydride transfer between molecules and the promotion of C−O bond scission, as shown mechanistically in Figure 13. This is the first radical reduction mechanism in heterogeneous catalysis below 200 °C.

Shi et al.[32] carried out mechanistic studies of FUR hydrogenation and hydrodeoxygenation of FUR to 2-MF and furan. Using DFT, they investigated the reaction energetics on a clean and hydrogen pre-covered hexagonal Mo_2C(101) surface. The mechanisms and the effect of hydrogen pressure on the selectivity were studied with a MKM, using the DFT data. The authors proposed that at hydrogen coverages of 0.25 ML, hydrogen adsorbs to all carbon sites, while the adsorption on Mo sites takes place at higher hydrogen partial pressures.

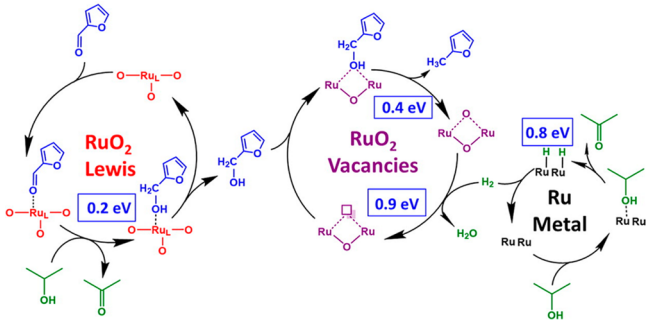

Figure 13. Proposed hydrogenolysis mechanism of FUR with a synergistic effect on Ru/RuO_2 sites with the corresponding values of highest energy barriers of the cycles. Reprinted with permission from ref 31. Copyright 2016 American Chemical Society.

In such case, FUR can only adsorb on neighboring Mo sites which suppresses its dissociation and promotes hydrogenation. According to *ab initio* atomistic thermodynamics, hydrogen coverage is proposed to be between 0.25 and 0.50 ML at temperatures between 400 and 600 K and pressures of 0.02−50 bar. The coverage of 0.25 ML was considered high and corresponds to reaction conditions at 423 K and 1 bar with a high H_2-to-FUR ratio (400:1). At these conditions, MKM shows that 2-MF is formed (up to 99%), while at lower hydrogen pressure furan is predominantly produced. The first activation barrier (dissociation) was found to be the rate- and selectivity-controlling step. The authors could not directly

DOI: 10.1021/acs.iecr.9b00898
Ind. Eng. Chem. Res. 2019, 58, 16018−16032

compare their results to experiments, but a comparison with the results from Lee et al.,[33] who used a Mo_2C catalyst in a flow reactor, showed good agreement. Therein, experimental selectivity toward 2-MF was reported to be ∼60%. Dimerization was also found to be important as the C_{10}+ compounds were produced with selectivities of up to 30%, while the rest was mostly FAL.

In the presence of Brønsted acids in aqueous media, furans can oligomerize. Nikbin et al.[72] computationally studied trimerization, using 2-MF as an example. The authors performed first-principles calculations of the activation barriers for individual reaction steps in a polarizable continuum solvent model (homogeneous catalysis) with the Zundel $H_5O_2^+$ complex as the reactive species. With a MKM based upon DFT calculation, it was shown that trimerization of 2-MF and self-polymerization of furan occur via ring hydrolysis and electrophilic aromatic substitution. However, 2,5-DMF cannot undergo oligomerization and instead converts into *p*-xylene. The reaction can be accelerated by lowering pH and increasing temperature.

Mironenko et al.[73] studied ring activation of furanic compounds on ruthenium catalysts. In a combined theoretical and experimental study, they performed DFT calculations, microkinetic modeling, and isotopic labeling experiments to elucidate the mechanism of H/D exchange and ring opening in various furanic molecules. They concluded that the H/D exchange of alkylated furans proceeds through ring opening. Only alkylated furans with unprotected α carbons (for instance 2-MF) are susceptible to the H/D exchange, while furan, FAL, and FUR are not. This mechanism is inconsistent with the Brønsted acid catalyzed ring activation. Instead, the sequence of C−O bond scission, dehydrogenation, deuteration, and ring closure constitutes the most probable reaction pathway.

Like 5-HMF and LA, furfural was studied mostly by DFT calculations, coupled with MKM. The most studied topic with furfural was the reaction selectivity toward hydrogenation or decarbonylation. The selectivity was found to be highly dependent on the orientation of adsorbed furfural; tilted adsorption leads to FAL, while flat adsorption leads to furan. The reaction can be greatly influenced by reaction condition. Hydrogen pressure and catalyst size (surface geometries) greatly influence selectivity, while hydrogen donor solvents and different surface sites (reduced/oxidized catalyst surface, vacancies) all actively participate in the reaction.

3. CONCLUSIONS

5-HMF, levulinic acid, and furfural are the most studied products of hemicellulose hydrolysis and conversion. 5-HMF, itself a fructose derivative, is encountered in the conversion of sugars into levulinic acid. Present multiscale studies focus mainly on the formation of 5-HMF. Several models account for the formation of possible side products, such as furfuryl alcohol, formic acid, or levulinic acid. When 5-HMF is further hydrodeoxygenated, DMF or eventually levulinic acid can form.

Levulinic acid is the product of furfural hydrogenation and its subsequent dehydration, accompanied by ring opening. Levulinic acid, itself possessing highly reactive carboxylic and oxo groups, can undergo a vast variety of different transformations upon hydrotreatment. Mostly, GVL and pentanoic acid are formed, although dimerization products are also detected.

Furfural is obtained with dehydration of C_5 sugars, which is formed in turn from hemicellulose hydrolysis. When hydrotreated, furfural is either hydrogenated into furfuryl alcohol or decarbonylated in furan. Generally, the selectivity is influenced primarily by hydrogen pressure and the corresponding hydrogen catalyst coverage. With larger hydrogen catalyst coverage, hydrogenation is favored. Further hydrogenation to 2-MF can proceed when an appropriate hydrogen donor is available, such as isopropanol. This reaction is especially efficient on multifunctional metal/metal oxide catalysts (for instance RuO_2/Ru), when C−O scission occurs even at low temperatures. Oligomerization is also possible when the medium is highly acidic and aqueous.

Lignocellulosic biomass is a ubiquitous renewable source of both energy and materials. In the past, biomass was mostly exploited for its caloric value. Combustion of biomass, although carbon neutral, has profound negative effects on the quality of air in the vicinity of domestic or industrial heaters on the account of PM emissions. Recently, biomass has been recognized also as a promising source for the production of added-value chemicals. Hemicellulose is an important constituent part of ligno-cellulosic biomass. As hemicellulose can be easily hydrolyzed to yield six-carbon and five-carbon sugars (hexoses and pentoses), which can be further converted into platform chemicals, it has been extensively studied already. However, research has been mostly limited to individual experimental and kinetic studies, while multiscale modeling has been neglected by most authors.

Multiscale modeling is still a nascent approach, with only seldom demonstrations in the literature. There are no studies of lignocellulosic biomass valorization with a full-fledged multiscale methodology approach, which would entail first-principles calculations, mesoscale simulations, and macroscale or reactor modeling. Mostly, studies are limited to experimental work, which is supplemented by microkinetic models as a confirmation tools. As these microkinetic models incorporate first-principles (DFT) data, they represent the first rung of multiscale modeling. Additionally, such models offer insight into the mechanism of reactions. Often only individual parts of reaction kinetics are studied, leaving comprehensive models still to be developed.

On one hand, multiscale modeling entails its own difficulties in implementation due to gaps between scales. On the other hand, this is a lively topic with different approaches still being developed and improved. In this Review, all multiscale and microkinetic approaches to computationally describe catalytic reactions for yielding the products of ligno-cellulosic biomass hydrolysis have finally been surveyed.

AUTHOR INFORMATION

Corresponding Authors

*E-mail: miha.grilc@ki.si.

*E-mail: matej.hus@ki.si.

ORCID

Miha Grilc: 0000-0002-8255-647X

Notes

The authors declare no competing financial interest.

ACKNOWLEDGMENTS

This research was funded by the Slovenian Research Agency (research core funding P2-0152 and basic postdoctoral research project Z2-9200). The work was partially carried out within the RDI project Cel. Cycle: "Potential of biomass for development of advanced materials and biobased products", which is co-financed by the Republic of Slovenia, Ministry of Education, Science and Sport, and the European Union through

DOI: 10.1021/acs.iecr.9b00898
Ind. Eng. Chem. Res. 2019, 58, 16018−16032

the European Regional Development Fund, 2016−2020. Authors also acknowledge Dr. Vili Resnik for his valuable comments and support during the revision of this work.

REFERENCES

(1) Besson, M.; Gallezot, P.; Pinel, C. Conversion of Biomass into Chemicals over Metal Catalysts. *Chem. Rev.* **2014**, *114* (3), 1827−1870.
(2) Climent, M. J.; Corma, A.; Iborra, S. Conversion of Biomass Platform Molecules into Fuel Additives and Liquid Hydrocarbon Fuels. *Green Chem.* **2014**, *16* (2), 516−547.
(3) Mika, L. T.; Cséfalvay, E.; Németh, Á. Catalytic Conversion of Carbohydrates to Initial Platform Chemicals: Chemistry and Sustainability. *Chem. Rev.* **2018**, *118* (2), 505−613.
(4) Mariscal, R.; Maireles-Torres, P.; Ojeda, M.; Sádaba, I.; López Granados, M. Furfural: A Renewable and Versatile Platform Molecule for the Synthesis of Chemicals and Fuels. *Energy Environ. Sci.* **2016**, *9* (4), 1144−1189.
(5) Chheda, J. N.; Huber, G. W.; Dumesic, J. A. Liquid-Phase Catalytic Processing of Biomass-Derived Oxygenated Hydrocarbons to Fuels and Chemicals. *Angew. Chem., Int. Ed.* **2007**, *46* (38), 7164−7183.
(6) Machado, G.; Leon, S.; Santos, F.; Lourega, R.; Dullius, J.; Mollmann, M. E.; Eichler, P. Literature Review on Furfural Production from Lignocellulosic Biomass. *Nat. Resour.* **2016**, *07* (03), 115−129.
(7) Girisuta, B.; Dussan, K.; Haverty, D.; Leahy, J. J.; Hayes, M. H. B. A Kinetic Study of Acid Catalysed Hydrolysis of Sugar Cane Bagasse to Levulinic Acid. *Chem. Eng. J.* **2013**, *217*, 61−70.
(8) Werpy, T.; Petersen, G. Top Value Added Chemicals from Biomass: Volume I−Results of Screening for Potential Candidates from Sugars and Synthesis Gas. *U.S. Dep. Energy* **2004**, DOI: 10.2172/15008859.
(9) Bozell, J. J.; Petersen, G. R. Technology Development for the Production of Biobased Products from Biorefinery Carbohydrates—the US Department of Energy's "Top 10" Revisited. *Green Chem.* **2010**, *12* (4), 539−554.
(10) Li, X.; Jia, P.; Wang, T. Furfural: A Promising Platform Compound for Sustainable Production of C_4 and C_5 Chemicals. *ACS Catal.* **2016**, *6*, 7621−7640.
(11) Salciccioli, M.; Stamatakis, M.; Caratzoulas, S.; Vlachos, D. G. A Review of Multiscale Modeling of Metal-Catalyzed Reactions: Mechanism Development for Complexity and Emergent Behavior. *Chem. Eng. Sci.* **2011**, *66* (19), 4319−4355.
(12) Vorotnikov, V.; Wang, S.; Vlachos, D. G. Group Additivity for Estimating Thermochemical Properties of Furanic Compounds on Pd(111). *Ind. Eng. Chem. Res.* **2014**, *53* (30), 11929−11938.
(13) Stamatakis, M.; Vlachos, D. G. Unraveling the Complexity of Catalytic Reactions via Kinetic Monte Carlo Simulation: Current Status and Frontiers. *ACS Catal.* **2012**, *2* (12), 2648−2663.
(14) Núñez, M.; Vlachos, D. G. Multiscale Modeling Combined with Active Learning for Microstructure Optimization of Bifunctional Catalysts. *Ind. Eng. Chem. Res.* **2019**, *58*, 6146.
(15) Eyring, H. The Activated Complex in Chemical Reactions. *J. Chem. Phys.* **1935**, *3* (2), 107−115.
(16) Mao, Y.; Wang, H.-F.; Hu, P. Theory and Applications of Surface Micro-Kinetics in the Rational Design of Catalysts Using Density Functional Theory Calculations. *Wiley Interdiscip. Rev.: Comput. Mol. Sci.* **2017**, *7* (6), No. e1321.
(17) Caratzoulas, S.; Vlachos, D. G. Converting Fructose to 5-Hydroxymethylfurfural: A Quantum Mechanics/Molecular Mechanics Study of the Mechanism and Energetics. *Carbohydr. Res.* **2011**, *346* (5), 664−672.
(18) Nikbin, N.; Caratzoulas, S.; Vlachos, D. G. A First Principles-Based Microkinetic Model for the Conversion of Fructose to 5-Hydroxymethylfurfural. *ChemCatChem* **2012**, *4* (4), 504−511.
(19) Asghari, F. S.; Yoshida, H. Kinetics of the Decomposition of Fructose Catalyzed by Hydrochloric Acid in Subcritical Water: Formation of 5-Hydroxymethylfurfural, Levulinic, and Formic Acids. *Ind. Eng. Chem. Res.* **2007**, *46* (23), 7703−7710.
(20) Yang, L.; Tsilomelekis, G.; Caratzoulas, S.; Vlachos, D. G. Mechanism of Brønsted Acid-Catalyzed Glucose Dehydration. *ChemSusChem* **2015**, *8* (8), 1334−1341.
(21) Gilkey, M. J.; Mironenko, A. V.; Yang, L.; Vlachos, D. G.; Xu, B. Insights into the Ring-Opening of Biomass-Derived Furanics over Carbon-Supported Ruthenium. *ChemSusChem* **2016**, *9* (21), 3113−3121.
(22) Grilc, M.; Likozar, B. Levulinic Acid Hydrodeoxygenation, Decarboxylation and Oligmerization over $NiMo/Al_2O_3$ Catalyst to Bio-Based Value-Added Chemicals: Modelling of Mass Transfer, Thermodynamics and Micro-Kinetics. *Chem. Eng. J.* **2017**, *330*, 383−397.
(23) Mamun, O.; Walker, E.; Faheem, M.; Bond, J. Q.; Heyden, A. Theoretical Investigation of the Hydrodeoxygenation of Levulinic Acid to γ-Valerolactone over Ru(0001). *ACS Catal.* **2017**, *7* (1), 215−228.
(24) Abdelrahman, O. A.; Heyden, A.; Bond, J. Q. Analysis of Kinetics and Reaction Pathways in the Aqueous-Phase Hydrogenation of Levulinic Acid To Form γ-Valerolactone over Ru/C. *ACS Catal.* **2014**, *4* (4), 1171−1181.
(25) Mamun, O.; Saleheen, M.; Bond, J. Q.; Heyden, A. Importance of Angelica Lactone Formation in the Hydrodeoxygenation of Levulinic Acid to γ-Valerolactone over a Ru(0001) Model Surface. *J. Phys. Chem. C* **2017**, *121* (34), 18746−18761.
(26) Wang, S.; Vorotnikov, V.; Vlachos, D. G. Coverage-Induced Conformational Effects on Activity and Selectivity: Hydrogenation and Decarbonylation of Furfural on Pd(111). *ACS Catal.* **2015**, *5* (1), 104−112.
(27) Sitthisa, S.; Pham, T.; Prasomsri, T.; Sooknoi, T.; Mallinson, R. G.; Resasco, D. E. Conversion of Furfural and 2-Methylpentanal on Pd/SiO_2 and $Pd−Cu/SiO_2$ Catalysts. *J. Catal.* **2011**, *280* (1), 17−27.
(28) Cai, Q.-X.; Wang, J.-G.; Wang, Y.-G.; Mei, D. Mechanistic Insights into the Structure-Dependent Selectivity of Catalytic Furfural Conversion on Platinum Catalysts. *AIChE J.* **2015**, *61* (11), 3812−3824.
(29) Pushkarev, V. V.; Musselwhite, N.; An, K.; Alayoglu, S.; Somorjai, G. A. High Structure Sensitivity of Vapor-Phase Furfural Decarbonylation/Hydrogenation Reaction Network as a Function of Size and Shape of Pt Nanoparticles. *Nano Lett.* **2012**, *12* (10), 5196−5201.
(30) Gilkey, M. J.; Panagiotopoulou, P.; Mironenko, A. V.; Jenness, G. R.; Vlachos, D. G.; Xu, B. Mechanistic Insights into Metal Lewis Acid-Mediated Catalytic Transfer Hydrogenation of Furfural to 2-Methylfuran. *ACS Catal.* **2015**, *5* (7), 3988−3994.
(31) Mironenko, A. V.; Vlachos, D. G. Conjugation-Driven "Reverse Mars−van Krevelen"-Type Radical Mechanism for Low-Temperature C−O Bond Activation. *J. Am. Chem. Soc.* **2016**, *138* (26), 8104−8113.
(32) Shi, Y.; Yang, Y.; Li, Y.-W.; Jiao, H. Mechanisms of $Mo_2C(101)$-Catalyzed Furfural Selective Hydrodeoxygenation to 2-Methylfuran from Computation. *ACS Catal.* **2016**, *6* (10), 6790−6803.
(33) Lee, W.-S.; Wang, Z.; Zheng, W.; Vlachos, D. G.; Bhan, A. Vapor Phase Hydrodeoxygenation of Furfural to 2-Methylfuran on Molybdenum Carbide Catalysts. *Catal. Sci. Technol.* **2014**, *4* (8), 2340−2352.
(34) Grote, A. F. V.; Tollens, B. Untersuchungen Über Kohlenhydrate. I. Ueber Die Bei Einwirkung von Schwefelsäure Auf Zucker Entstehende Säure (Levulinsäure). *Justus Liebigs Ann. Chem.* **1875**, *175* (1−2), 181−204.
(35) Yu, I. K. M.; Tsang, D. C. W. Conversion of Biomass to Hydroxymethylfurfural: A Review of Catalytic Systems and Underlying Mechanisms. *Bioresour. Technol.* **2017**, *238*, 716−732.
(36) Moreau, C.; Finiels, A.; Vanoye, L. Dehydration of Fructose and Sucrose into 5-Hydroxymethylfurfural in the Presence of 1-H-3-Methyl Imidazolium Chloride Acting Both as Solvent and Catalyst. *J. Mol. Catal. A: Chem.* **2006**, *253* (1−2), 165−169.

DOI: 10.1021/acs.iecr.9b00898
Ind. Eng. Chem. Res. 2019, 58, 16018−16032

(37) Assary, R. S.; Redfern, P. C.; Hammond, J. R.; Greeley, J.; Curtiss, L. A. Computational Studies of the Thermochemistry for Conversion of Glucose to Levulinic Acid. *J. Phys. Chem. B* **2010**, *114* (27), 9002−9009.
(38) Assary, R. S.; Kim, T.; Low, J. J.; Greeley, J.; Curtiss, L. A. Glucose and Fructose to Platform Chemicals: Understanding the Thermodynamic Landscapes of Acid-Catalysed Reactions Using High-Level Ab Initio Methods. *Phys. Chem. Chem. Phys.* **2012**, *14* (48), 16603−16611.
(39) Kramers, H. A. Brownian Motion in a Field of Force and the Diffusion Model of Chemical Reactions. *Physica* **1940**, *7* (4), 284−304.
(40) Grote, R. F.; Hynes, J. T. Energy Diffusion-controlled Reactions in Solution. *J. Chem. Phys.* **1982**, *77* (7), 3736−3743.
(41) Girisuta, B.; Janssen, L. P. B. M.; Heeres, H. J. Green Chemicals: A Kinetic Study on the Conversion of Glucose to Levulinic Acid. *Chem. Eng. Res. Des.* **2006**, *84* (5), 339−349.
(42) Pilath, H. M.; Nimlos, M. R.; Mittal, A.; Himmel, M. E.; Johnson, D. K. Glucose Reversion Reaction Kinetics. *J. Agric. Food Chem.* **2010**, *58* (10), 6131−6140.
(43) Weingarten, R.; Cho, J.; Xing, R.; Conner, W. C.; Huber, G. W. Kinetics and Reaction Engineering of Levulinic Acid Production from Aqueous Glucose Solutions. *ChemSusChem* **2012**, *5* (7), 1280−1290.
(44) Jae, J.; Zheng, W.; Lobo, R. F.; Vlachos, D. G. Production of Dimethylfuran from Hydroxymethylfurfural through Catalytic Transfer Hydrogenation with Ruthenium Supported on Carbon. *ChemSusChem* **2013**, *6* (7), 1158−1162.
(45) Luo, J.; Arroyo-Ramírez, L.; Wei, J.; Yun, H.; Murray, C. B.; Gorte, R. J. Comparison of HMF Hydrodeoxygenation over Different Metal Catalysts in a Continuous Flow Reactor. *Appl. Catal., A* **2015**, *508*, 86−93.
(46) Kumalaputri, A. J.; Bottari, G.; Erne, P. M.; Heeres, H. J.; Barta, K. Tunable and Selective Conversion of 5-HMF to 2,5-Furandimethanol and 2,5-Dimethylfuran over Copper-Doped Porous Metal Oxides. *ChemSusChem* **2014**, *7* (8), 2266−2275.
(47) Román-Leshkov, Y.; Barrett, C. J.; Liu, Z. Y.; Dumesic, J. A. Production of Dimethylfuran for Liquid Fuels from Biomass-Derived Carbohydrates. *Nature* **2007**, *447* (7147), 982−985.
(48) Patet, R. E.; Nikbin, N.; Williams, C. L.; Green, S. K.; Chang, C.-C.; Fan, W.; Caratzoulas, S.; Dauenhauer, P. J.; Vlachos, D. G. Kinetic Regime Change in the Tandem Dehydrative Aromatization of Furan Diels−Alder Products. *ACS Catal.* **2015**, *5* (4), 2367−2375.
(49) Patet, R. E.; Koehle, M.; Lobo, R. F.; Caratzoulas, S.; Vlachos, D. G. General Acid-Type Catalysis in the Dehydrative Aromatization of Furans to Aromatics in H-[Al]-BEA, H-[Fe]-BEA, H-[Ga]-BEA, and H-[B]-BEA Zeolites. *J. Phys. Chem. C* **2017**, *121* (25), 13666−13679.
(50) Green, S. K.; Patet, R. E.; Nikbin, N.; Williams, C. L.; Chang, C.-C.; Yu, J.; Gorte, R. J.; Caratzoulas, S.; Fan, W.; Vlachos, D. G.; et al. Diels−Alder Cycloaddition of 2-Methylfuran and Ethylene for Renewable Toluene. *Appl. Catal., B* **2016**, *180*, 487−496.
(51) Hočevar, B.; Grilc, M.; Huš, M.; Likozar, B. Mechanism, Ab Initio Calculations and Microkinetics of Hydrogenation, Hydrodeoxygenation, Double Bond Migration and Cis−trans Isomerisation during Hydrotreatment of C_6 Secondary Alcohol Species and Ketones. *Appl. Catal., B* **2017**, *218*, 147−162.
(52) Hočevar, B.; Grilc, M.; Huš, M.; Likozar, B. Mechanism, Ab Initio Calculations and Microkinetics of Straight-Chain Alcohol, Ether, Ester, Aldehyde and Carboxylic Acid Hydrodeoxygenation over Ni-Mo Catalyst. *Chem. Eng. J.* **2019**, *359*, 1339−1351.
(53) Kougioumtzis, M. A.; Marianou, A.; Atsonios, K.; Michailof, C.; Nikolopoulos, N.; Koukouzas, N.; Triantafyllidis, K.; Lappas, A.; Kakaras, E. Production of 5-HMF from Cellulosic Biomass: Experimental Results and Integrated Process Simulation. *Waste Biomass Valorization* **2018**, *9* (12), 2433−2445.
(54) Rackemann, D. W.; Doherty, W. O. The Conversion of Lignocellulosics to Levulinic Acid. *Biofuels, Bioprod. Biorefin.* **2011**, *5* (2), 198−214.
(55) Jing, Q.; Lü, X. Kinetics of Non-Catalyzed Decomposition of Glucose in High-Temperature Liquid Water. *Chin. J. Chem. Eng.* **2008**, *16* (6), 890−894.
(56) Tarabanko, V. E.; Chernyak, M. Y.; Aralova, S. V.; Kuznetsov, B. N. Kinetics of Levulinic Acid Formation from Carbohydrates at Moderate Temperatures. *React. Kinet. Catal. Lett.* **2002**, *75* (1), 117−126.
(57) Chang, C.; Ma, X.; Cen, P. Kinetics of Levulinic Acid Formation from Glucose Decomposition at High Temperature. *Chin. J. Chem. Eng.* **2006**, *14* (5), 708−712.
(58) Girisuta, B.; Danon, B.; Manurung, R.; Janssen, L. P. B. M.; Heeres, H. J. Experimental and Kinetic Modelling Studies on the Acid-Catalysed Hydrolysis of the Water Hyacinth Plant to Levulinic Acid. *Bioresour. Technol.* **2008**, *99* (17), 8367−8375.
(59) Chang, C.; Ma, X.; Cen, P. Kinetic Studies on Wheat Straw Hydrolysis to Levulinic Acid. *Chin. J. Chem. Eng.* **2009**, *17* (5), 835−839.
(60) Tan-Soetedjo, J. N. M.; van de Bovenkamp, H. H.; Abdilla, R. M.; Rasrendra, C. B.; van Ginkel, J.; Heeres, H. J. Experimental and Kinetic Modeling Studies on the Conversion of Sucrose to Levulinic Acid and 5-Hydroxymethylfurfural Using Sulfuric Acid in Water. *Ind. Eng. Chem. Res.* **2017**, *56* (45), 13228−13239.
(61) Fachri, B. A.; Abdilla, R. M.; van de Bovenkamp, H. H.; Rasrendra, C. B.; Heeres, H. J. Experimental and Kinetic Modeling Studies on the Sulfuric Acid Catalyzed Conversion of d -Fructose to 5-Hydroxymethylfurfural and Levulinic Acid in Water. *ACS Sustainable Chem. Eng.* **2015**, *3* (12), 3024−3034.
(62) Qing, Q.; Guo, Q.; Wang, P.; Qian, H.; Gao, X.; Zhang, Y. Kinetics Study of Levulinic Acid Production from Corncobs by Tin Tetrachloride as Catalyst. *Bioresour. Technol.* **2018**, *260*, 150−156.
(63) Braden, D. J.; Henao, C. A.; Heltzel, J.; Maravelias, C. C.; Dumesic, J. A. Production of Liquid Hydrocarbon Fuels by Catalytic Conversion of Biomass-Derived Levulinic Acid. *Green Chem.* **2011**, *13* (7), 1755−1765.
(64) Abdelrahman, O. A.; Heyden, A.; Bond, J. Q. Microkinetic Analysis of C_3−C_5 Ketone Hydrogenation over Supported Ru Catalysts. *J. Catal.* **2017**, *348*, 59−74.
(65) Abdelrahman, O. A.; Luo, H. Y.; Heyden, A.; Román-Leshkov, Y.; Bond, J. Q. Toward Rational Design of Stable, Supported Metal Catalysts for Aqueous-Phase Processing: Insights from the Hydrogenation of Levulinic Acid. *J. Catal.* **2015**, *329*, 10−21.
(66) Bond, J. Q.; Jungong, C. S.; Chatzidimitriou, A. Microkinetic Analysis of Ring Opening and Decarboxylation of γ-Valerolactone over Silica Alumina. *J. Catal.* **2016**, *344*, 640−656.
(67) Chung, Y.-H.; Peng, T.-H.; Lee, H.-Y.; Chen, C.-L.; Chien, I.-L. Design and Control of Reactive Distillation System for Esterification of Levulinic Acid and *n* -Butanol. *Ind. Eng. Chem. Res.* **2015**, *54* (13), 3341−3354.
(68) Kokare, M. B.; V, R.; Mathpati, C. S. Response Surface Optimization, Kinetic Study and Process Design of n-Butyl Levulinate Synthesis. *Chem. Eng. Res. Des.* **2018**, *137*, 577−588.
(69) Wang, S.; Vorotnikov, V.; Vlachos, D. G. A DFT Study of Furan Hydrogenation and Ring Opening on Pd(111). *Green Chem.* **2014**, *16* (2), 736−747.
(70) Lyu, J.; Wang, J.; Lu, C.; Ma, L.; Zhang, Q.; He, X.; Li, X. Size-Dependent Halogenated Nitrobenzene Hydrogenation Selectivity of Pd Nanoparticles. *J. Phys. Chem. C* **2014**, *118* (5), 2594−2601.
(71) Crespo-Quesada, M.; Yarulin, A.; Jin, M.; Xia, Y.; Kiwi-Minsker, L. Structure Sensitivity of Alkynol Hydrogenation on Shape- and Size-Controlled Palladium Nanocrystals: Which Sites Are Most Active and Selective? *J. Am. Chem. Soc.* **2011**, *133* (32), 12787−12794.
(72) Nikbin, N.; Caratzoulas, S.; Vlachos, D. G. On the Oligomerization Mechanism of Brønsted Acid-Catalyzed Conversion of Furans to Diesel-Range Fuels. *Appl. Catal., A* **2014**, *485*, 118−122.
(73) Mironenko, A. V.; Gilkey, M. J.; Panagiotopoulou, P.; Facas, G.; Vlachos, D. G.; Xu, B. Ring Activation of Furanic Compounds on Ruthenium-Based Catalysts. *J. Phys. Chem. C* **2015**, *119* (11), 6075−6085.

DOI: 10.1021/acs.iecr.9b00898
Ind. Eng. Chem. Res. 2019, 58, 16018−16032